	Experiment title: **Investigation of Electric Field Induced structural modifications in BaTiO₃ ferroelectric and Sr₁₋ₓPrₓTiO₃ relaxor ferroelectric compounds at different scale lengths**	**Experiment number**: HC-2330
Beamline: ID22	**Date of experiment**: from: 21/09/2016 to: 26/09/2016	**Date of report**: 21.08.2020
Shifts: 15	**Local contact(s):** Carlotta Giacobbe	*Received at ESRF:*

Names and affiliations of applicants (* indicates experimentalists):

Marco Scavini*, Stefano Checchia*, Mattia Allieta
Università degli Studi di Milano, Dip. di Chimica, Milano, Italy;

Riccardo Cabassi*
ᶜCNR-IMEM, Parco Area delle Scienze, 37/A, 43124 Parma, Italy

Claudio Ferrero*, Mauro Coduri*
ESRF

Report

Experiment HC-2330 at ID22 investigated the electric-field induced macroscopic and microscopic structural evolution of ferroelectric BaTiO₃ and Relaxor ferroelectric Sr₁₋ₓPrₓTiO₃ titanates, performing high resolution powder diffraction and pair distribution function experiments at different amplitudes of applied dc electric field, in order to reveal differences and similarities in the response of different classes of materials.

Being the first experiment under electric field made by the proponent group great attention was given to the development of the sample environment.

1. Scientific Background

The prototypical ferroelectric perovskite BaTiO₃ at temperature T_c, undergoing transition between its paraelectric and the FE phases, exhibits a sharp frequency-independent divergence of the dielectric constant ε. At the same temperature a structural transition take place from centrosymmetric $Pm\bar{3}m$ to polar $P4mm$ space groups. At the atomic scale, this transition corresponds to the shift of the Ti position away from the center of its octahedral oxygen cage so producing an electric dipole.

Relaxor ferroelectrics, by contrast, exhibit a broad, frequency dependent peak of ε at T_c and no break of centrosymmetry in the average structure. Some centrosymmetric phases were shown to approach FE behaviour while maintaining their centrosymmetric structure even below the transition. This is the case of Pr doped strontium titanate (Sr₁₋ₓPrₓTiO₃): its dielectric peak is present around T_C=500 K in the $0 < x \le 0.15$ range, while

an undistorted perovskite cubic structure is maintained below T_C. A structural transition toward the centrosymmetric $I4/mcm$ space group sets in at lower temperatures, signalling the occurrence of polar nanoregions, revealed at the local scale to merge to a centrosymmetric structure on average.**[Checchia16]**

The macroscopic structural effects reflect smaller-scale local atomic displacements, nanoscale polarization reversal (domain switching) and movement of domain walls (DW) greatly affecting the microstructure in polycrystalline materials.

Crystallography under electric field has been recently applied to reveal these macroscopic and microscopic structural response of piezo/ferro-electric materials to intense electric fields.

In HC2330 we focused on the crystallographic structure of two systems: pure and Eu-doped $BaTiO_3$ FE materials and the occupationally disordered relaxor ferroelectric oxide $Sr_{0.85}Pr_{0.15}TiO_3$. As to the latter system, while its centrosymmetric structure should inhibit long-range polarization, its relaxor properties point to local polar fluctuations and a host of possible structural changes on applying **E**.

2. Experimental

2.1 Samples

Samples of $Sr_{0.85}Pr_{0.15}TiO_3$ and $SrTiO_3$ were synthetized as described in Ref.**[Checchia16]**. In the last firing cycle, pellets as thick as 0.3 mm here heated at 1673 K for 4 hours. The cylindrical shaped pellets (diameter = 5mm, thickness ≈ 0.3 mm) were metallized (few tens of nm thick) with gold.

The very high T values during final firing step were selected to induce the growth of large crystallites so minimizing the contribution of the microstructure to the macroscopic electric behaviour.


2.2 Experimental Cell for XRPD measurements under electric field

For Rietveld quality measurements, samples were put between two glassy slides and mounted on the high E-field cell depicted in Figure 1A (DeltaE s.r.l.). Electric contacts were guaranteed by ITO films sputtered on the slides and by carbon cloths pellets inserted to obtain the correct thickness. The measure cell was fastened onto a steel support with suitable rotational degrees of freedom to allow rotation of the entire cell around an Ω axis coaxial to the 2θ one.

The system geometries are sketched in Fig.1B. Two angles are reported in the figure: Ω between the direction of the incident beam and the normal to the pellet surface and α between **E** and the scattering vector **Q**. While Ω was kept constant during each measurements, α varied on changing 2θ angle: α =90°-Ω-θ. In Fig.1B are reported the α intervals corresponding to the investigated 2θ range for each Ω adopted.
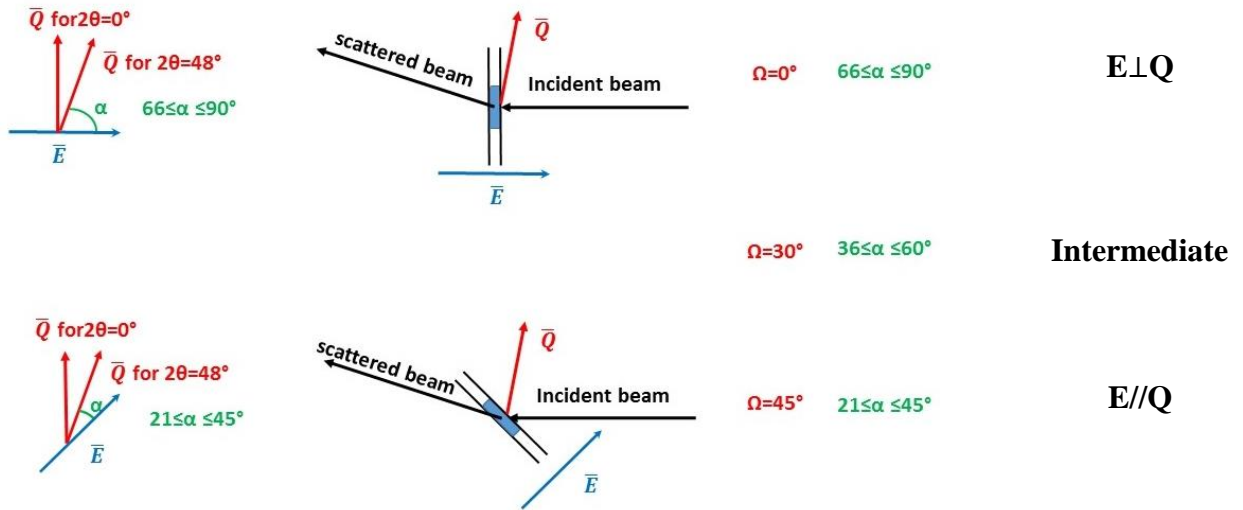
For PDF quality measurements we adopted a different cell, described in detail in **[Daniels09]** because the geometry of theprevious cell inhibited measurements at the high 2θ values (and Q alues) needed for PDF. For Ω =0° the electric field was perpendicular to the incident beam and directed along the y axis of the diffractometer (i.e. perpendicular to the ground floor)
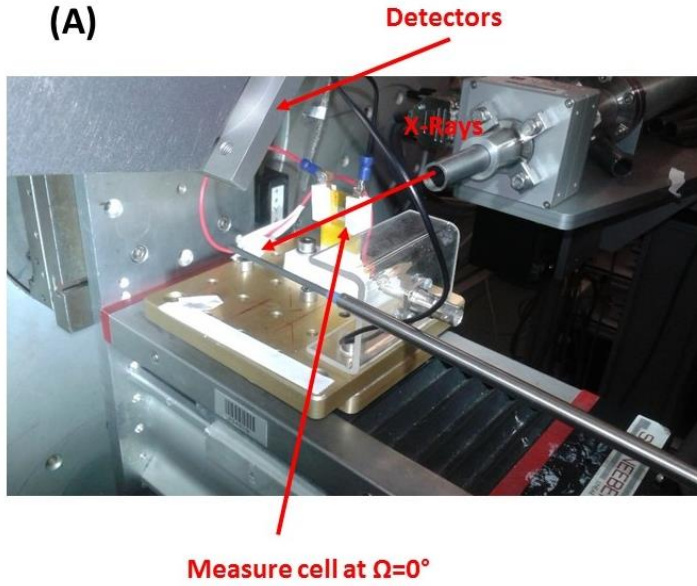
Figure 1. (A) Photograph of the measure cell and scheme of the ITO electrodes. (B) Sketch of the collection geometries varying the angle Ω between the incident beam and the electric field direction. Only geometries for Ω=0 and 45° are depicted in the figure. The angle α between the scattering vector and the electric field directions is also shown together to the angle intervals while scanning 2θ from 0 to 48°. Minimum α value correspond to maximum 2θ and *vice versa*.

The angle α between **E** and the scattering vector **Q** varied in the 66≤α≤90°, 36≤α≤60° and 21≤α≤45° ranges respectively, during the scans as sketched in Fig.1B, from top to bottom. In the following, we will call these three geometries as "E perpendicular to Q" (**E⊥Q**), "intermediate" and "E parallel to Q" (**E//Q**), respectively for sake of semplicity, as shown in the right part of Fig.1B

2.3 XRPD Data collection

Rietveld quality XRPD measurements on $Sr_{0.85}Pr_{0.15}TiO_3$ pellets were collected in transmission mode at room temperature using a high-resolution setup, an X-ray wavelength λ=0.354292(6) Å and a 9-element detector array in the 0≤ 2θ ≤48° interval (Q_{max}=14.4 Å^{-1}), 2 °/min for a total counting time of 20 min/pattern.

Patterns were collected at three different angles Ω =0, 30 and 45° (in sequence) between the electric field **E** and the incident beam directions. The angle α between **E** and the scattering vector **Q** varied in the 66≤α≤90°, 36≤α≤60° and 21≤α≤45° ranges respectively, during the scans as sketched in Fig.1B. In the following, we will call these three geometries as E perpendicular to Q (**E⊥Q**), intermediate and E parallel to Q (**E//Q**), respectively for sake of semplicity.

Measurements were carried out first at zero field at all Ω angles. Then, the same data collection was applied at 100, 500, 1000 V. After that, the electric field was turned off and a complete set of data was collect at zero field to check forpossible hysteresis effects. Sets of measurements at 1500 and 2000 V were finally acquired. Due to the geometry of the pellets this correponds applied electric field up to 6 kV/mm.

In the geometry of the cell used for PDF **[Daniels09]**, in the high-resolution setup, we adopted θ/2θ collection strategy: **E** and **Q** were always parallel to each other in the vertical scattering plane.

For PDF analysis of the $Sr_{0.85}Pr_{0.15}TiO_3$ sample, a wider 2θ range (0-98°) was investigates using the same HR-setup, increasing the counting time on increasing the diffraction angle for a total counting time of 6 hours to reach suitable Q range (up to ≈ 25 Å^{-1}) and signal to noise ratio for PDF.

3. Results:

3.1 Direct analysis of Bragg Peaks

The direct analysis of Bragg Peaks focused on the peaks of the $(h00)_P$ $(hh0)_P$ and $(hhh)_P$ families, where the subscript "P" indicates that indexing follows the perovskite cubic setting. In the tetragonal phase of of $Sr_{0.85}Pr_{0.15}TiO_3$ the first two families split into $(00h)_P < [(h00)_P \equiv (0h0)_P]$ and $(hh0)_P < [(h0h)_P \equiv (0hh)_P]$ doublets respectively, where the symbols < indicate that the former peak family appear at lower 2θ then the latter values because $a_T < c_T$.
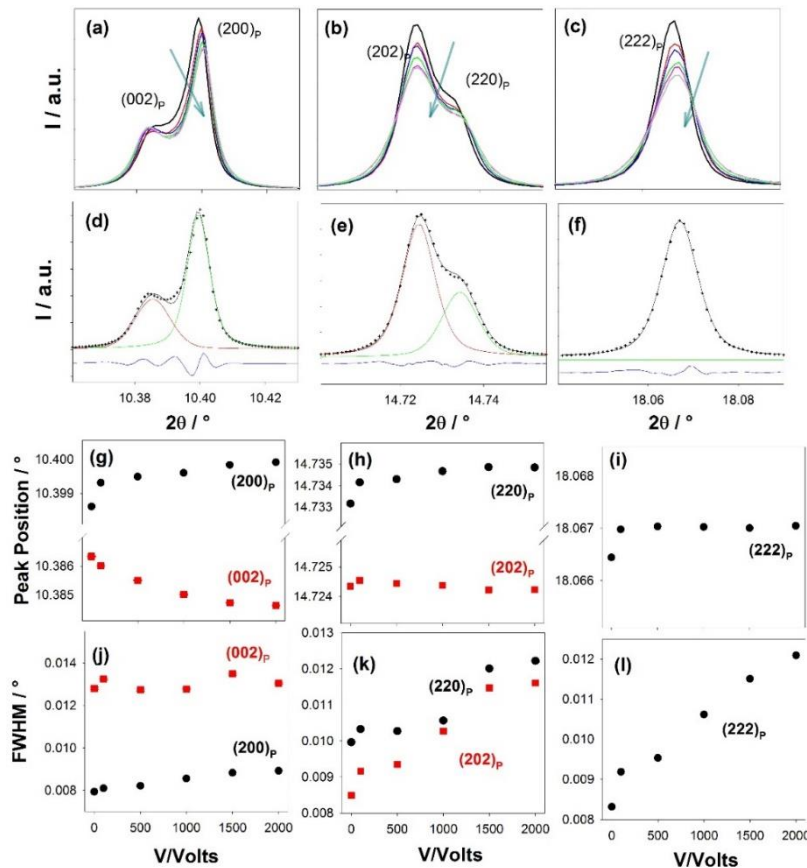
Figure 2. (a-c) selected experimental diffraction peaks of $Sr_{0.85}Pr_{0.15}TiO_3$ at different V values in the 0-2000 V range. Numbers into brackets are the pertinent miller indexes in the perovskite setting. Cyan arrows indicate increasing applied voltage. (d-f) Fits of the same diffraction peaks at V = 500 V, using pseudo-voigt functions. (g-i) Positions and (j-l) FWHM of the same peaks of panels (a-c).

In panels (a)-(c) Figure 2 are reported the plots of $(200)_P$ $(220)_P$ and $(222)_P$ peaks at different V values and $\Omega=0$. On increasing V, most peaks broaden and change their position, suggesting that the applied electric field induces microscopic (inhomogeneous) strain in the structure. At the same time, some peaks shift their position indicating that also macroscopic (homogeneous) strain is induced by E. Finally, the relative intensity of couples of peaks (e.g. $(002)_P/(200)_P$ doublets) changes on poling suggesting some texture effect.

In panels (d)-(f) of Fig.2 are reported as examples the refinements of the same peaks for V=500 V, using pseudo-Voigt functions . As to the $(002)_P/(200)_P$ doublet, the modulated shape of the residual reveals some systematic deviation from the model adopted for the fit, due to the (hkl) dependent asymmetry of the two peaks. The $(002)_P$ and $(200)_P$ peaks show a broader tail on their right and left side, respectively.

This asymmetry has been observed in pure and slightly doped tetragonal $BaTiO_3$ (*P4mm*) **[Darlington91]** and in $Pb(Zr,Nb)O_3$ **[Kisi08]** as well as in variously doped PZT [Pramanick09] and were attributed to stresses along or strain within domain walls DW. The fitted peak positions and the full widths at half maximum (FWHM) parameters are reported versus V in panels (g)-(l) of Fig.2 for the same reflections.

3.2 Rietveld analysis

The $Sr_{0.85}Pr_{0.15}TiO_3$ sample is tetragonal *I4/mcm* in the whole E range, in line with zero field, room-temperature **[Checchia16]**, i.e. no polar phase is formed under **E**. With respect to the perovskite cubic cell TiO_6 octahedra are tilted along the c-axis in a antiferrodistorsive (AFD) pattern so inducing the doubling of the c axis ($\mathbf{c}_T=2\mathbf{c}_P$) while the tetragonal $\mathbf{a}_T$ and $\mathbf{b}_T$ axis originate from the cubic perovskite ones $\mathbf{a}_P$, $\mathbf{b}_P$, $\mathbf{c}_P$ applying the following vector sums: $\mathbf{a}_T=\mathbf{a}_P+\mathbf{b}_P$; $\mathbf{b}_T=\mathbf{a}_P-\mathbf{b}_P$. We can define the tetragonal strain η as $(c_P/a_P)-1$ [$\equiv 2(c_T/\sqrt{2}a_T)-1$]where a_T and c_T are the moduli of the tetragonal cell vectors and a_P and c_P are in pseudocubic setting. The tilting of octahedral causes the split of the oxygen site into two non equivalent ones: the *apical* O1 site which lies on the tilting axis at (0, 0, ¼) and the *equatorial* O2 one at (x, x+½, 0). The tilting angle ϕ depends only on x(O2) and is calculated following the equation $\tan\phi =1-4\ x$(O2) **[Allieta12]**; for x(O2)=0.25, $\phi=0$: the oxygen ions sit on the same sites as in the cubic cell.

A)

B)
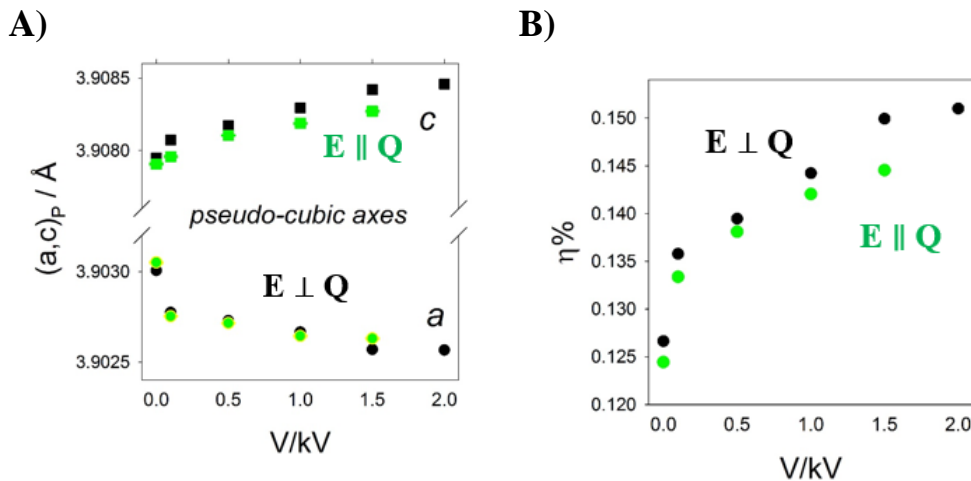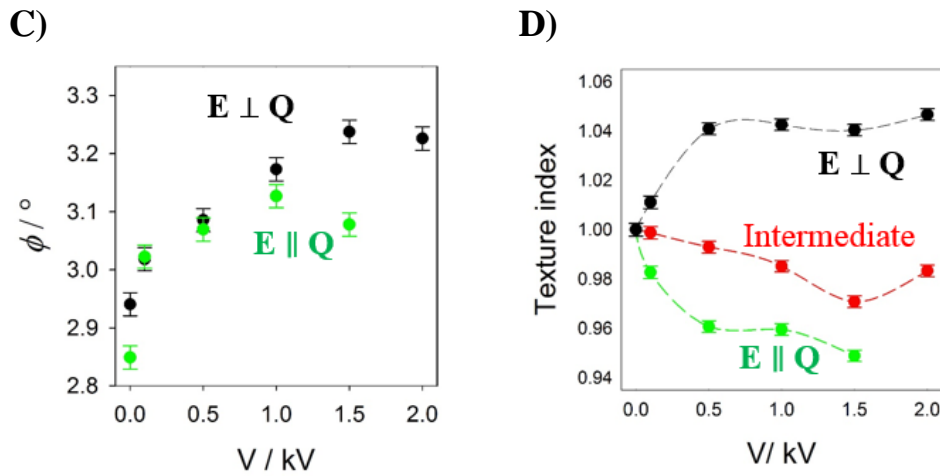
Figure 3. Fitted Rietveld parameters vs. V. A) pseudo-cubic cell constants a (circles) and c (squares). B) tetragonal strain. C) Tilting angle φ; D: Texture parameters; Black, red and green symbols refer to Ω=0, 30 and 45° (black, red and blue circles, respectively).

The results of the Rietveld refinement confirm the direct analysis shown above. In particular, the macroscopic strain parameter η is affected by poling: this corresponds to the converse piezoelectric effect.

Also the tilting angle value is affected by the electric field. Finally, the changes in the relative intensity revealed by the direct analysis corresponds to the texture index variation of the Rietveld Refinement.

In the centrosymmetric $I4/mcm$ phase no polar axis exists. However, even our refinements evidenced changes in the texture parameters vs. the applied field and Ω angle: Fig.3D suggests that in all cases the volume of domains with the c axis perpendicular (parallel) to **E** grows (shrink). Coupled to the increased homogeneous and inhomogeneous strain and to the changes in the tilting angle values, it suggest some interplay between FE and AFD instabilities in Pr-doped SrTiO$_3$, as the applied fields induce movements of the 90° domain walls.

3.3 PDF analysis

Two PDF-quality patterns have been collected on a new Sr$_{0.85}$Pr$_{0.15}$TiO$_3$ pellet before poling and applying V=1.5 kV..

Figure 4A shows the two G(r) functions in a wide r range, as black (V=0, hereafter G(r)$_{0V}$) and red (V=1.5 kV, hereafter G(r)$_{1.5kV}$) curves. Figs.4B and 4C report portions of the same G(r) at low and high r values, respectively. At low r values, the first interatomic distances in perovskite titanates differ enough one another to allow unique labelling. In Fig.4B the 1st Sr/Pr-O distances lie at $r \approx 2.70$ Å, followed by the 1st Sr/Pr-Ti one at $r \approx 3.37$ Å, while the Sr/Pr-Sr/Pr plus Ti-Ti distances around $r \approx 3.90$ Å correspond to the pseudo-cubic cell edge. Between 4 and 5 Å, the 2nd Ti-O (≈ 4.40 Å) and Sr/Pr-O (≈ 4.80 Å) contacts appear, followed by further cation-cation distances. Small differences between the two curves arise for cation-cation peaks. Conversely, sizable changes appear in correspondence to the cation-oxygen distances, in particular, in the 2-3 and 4-5 Å intervals as displayed in Fig.4B.
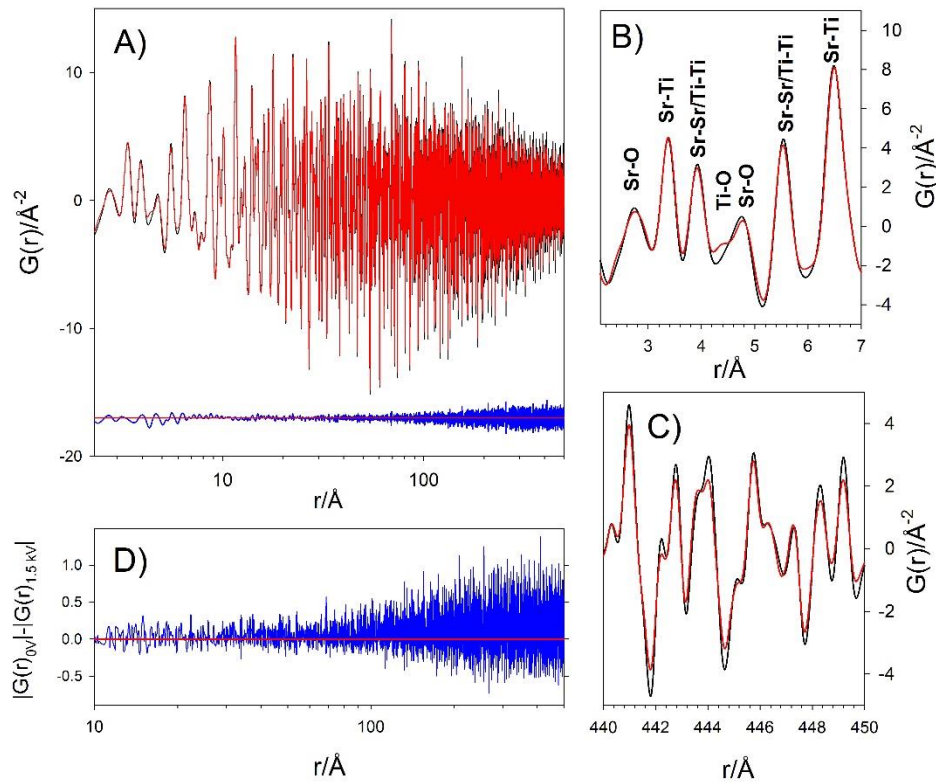
Figure 4. A) Experimental G(r) functions collected before applying the electric filed (black trace) and under V= 1500 V. B) and C) details of the same curves; D) Difference between the absolute values of the two curves ΔG'=|G(r)$_{0V}$| - |G(r)$_{1.5kV}$| in the 10-500 Å interval

While at intermediate *r* (10-30 Å) the differences between the two curves are negligible, (Figure 4D)at larger interatomic distances the magnitude of their difference increases constantly with *r*. As shown in Fig. 4C for a small region of both G(r)s at very high *r* ranges, peak amplitude is smaller when the electric field is applied. To evidence this effect, in panel D) of Fig.4 is reported the function $|G(r)_{0V}| - |G(r)_{1.5kV}|$ vs *r*, for r>10 Å: in case of mere peak mismatch without damping of peaks amplitudes, the barycenter of this function should be zero as in the blue curve of panel A. The excess of positive values of this trace points to dampening of $G(r)_{1.5kV}$ induced by the electric field starting from ≈30-40 Å. This finding matches with the Bragg peak broadening observed above, which was assigned to increasing inhomogeneous strain.

The two G(r) functions have been fitted using the so called Real Space Rietveld analysis revealing that poling raises local polar distorton strictly related to the defect chemistry of this compound, which, in turn, cause the (in)homogeneous strain, the <u>converse piezoelectric effect</u> and the domain walls movements detected by the reciprocal spaces analysis.

References

[Allieta12] M. Allieta, M. Scavini, L. Spalek, V. Scagnoli, H. Walker, C. Panagopoulos, S. Saxena, T. Katsufuji and C. Mazzoli. Role of intrinsic disorder in the structural phase transition of magnetoelectric EuTiO$_3$. **Physical Review B85**, (2012) 184107

[Checchia16] S. Checchia, M. Allieta, M. Coduri, M. Brunelli, M. Scavini. Relaxor ferroeletric behavior in Sr$_{1-x}$Pr$_x$TiO$_3$: cooperation between polar and antiferrodistortive instabilities. Physical Review **B, 94** (2016) 104201 1-8.

[Daniels09] J. Daniels, A. Pramanick, J.L. Jones. Time-resolved X-ray diffraction characterization of ferroelectrics. IEEE Transactions on Ultrasonics, Ferroelectrics, and Frequency Control, **56** (2009) 1539-45, DOI: 10.1109/TUFFC.2009.1218

[Darlington91] C.N.W. Darlington, R.J. Cernik. The ferroelectric phase transition in pure and lightly doped barium titanate. J.Phys.: Condens. Matter **3** (1991) 4555-67.

[Kisi08] Erich H. Kisi, Christopher J. Howard, Applications of Neutron Powder Diffraction, Oxford University Press Inc., New York (2008) ISBN 978–0–19–851594–4

[Pramanick09] A. Pramanick, J. Daniels, J.L. Jones, J. Am. Ceram. Soc., 92 (2009) 2300-10, Subcoercive electrical loading of Lead Zirconate Titanate Ceramics II: Time-resolved X-ray diffraction. DOI: 10.1111/j.1551-2916.2009.03219.x

.